MicroPEPT: A step towards hybrid PEPT detectors

R van der Merwe*, S Peterson, A Buffler, M van Heerden, A McKnight and T Leadbeater

Department of Physics, University of Cape Town, South Africa

E-mail: * VMRROB003@myuct.ac.za

Abstract. Positron Emission Particle Tracking (PEPT) measures the trajectory of a freely moving radioactive tracer particle, and enables the non-invasive study of dynamic systems from engineering to medicine. PEPT performance is limited by the activity achievable in radiolabelling a suitable tracer particle, and the fixed geometry of conventional detector systems. In investigating phenomena on micro-scales, recent development of advanced instrumentation has been required to offset these limitations. A modular bismuth germanate oxide (BGO) scintillator array, with detection modules derived from CTI/Siemens PET scanners, has been constructed and coupled to a recently developed data acquisition system. This array consists of 1024 detector elements (512 pixels of 6.75 x 6.25 x 30 mm and 512 pixels of 4.1 x 4.0 x 30 mm) giving a field of view of 150 mm x 196 mm x 101 mm. Energy and timing resolutions of this system were determined and sensitivity profiles were modelled numerically, informing on optimal system parameters to enable future characterisation of the detector efficiency, spatial resolution and deadtime parameters. These initial results indicate the applicability of modular BGO scintillator arrays in addressing small scale flow phenomena, and lead the direction of future work in combining the BGO system with a pair of high resolution pixelated semiconductor detectors for the first time.

1. Introduction

The Positron Emission Particle Tracking (PEPT) technique can be used to non-invasively study dynamic systems, with applications in fields from engineering to medicine [1, 2, 3]. By radiolabeling a suitable tracer particle, tracking can be performed to high spatial and temporal resolution over an extended time, from which the trajectory of the tracer can be determined with an associated uncertainty. Recently, a need to examine more challenging systems on the micro-scale has arisen with PEPT applications in the study of micro-scale flows, such as the flows in biological systems and microfluidic devices, as well as potential applications in beam line tracking in proton radiotherapy [4]. However, PEPT performance of existing systems is limited by the absolute efficiencies of fixed geometries, compounded by low activity in radiolabeling suitable small tracer particles, leading to the requirement of advanced instrumentation development. Previous work with semiconductor detectors has demonstrated the feasibility of applying PEPT to micro-scale systems [4], but the achievable field-of-view (FOV) and location rates were limiting, promoting the benefits of development towards a hybrid detection system accounting for these limitations. In this paper, the development and characterization of a modular scintillator array designed to support a semiconductor detection system is performed, serving as a first step towards the development of hybrid detection systems optimised for micro-scale particle tracking.

2. The PEPT technique and spatial resolution

The PEPT technique makes use of proton rich radioisotopes to label a suitable tracer particle for the system of interest. Emitted positrons annihilate with free electrons to produce two approximately back-to-back 511 keV photons due to momentum conservation [5]. When these photons are detected in coincidence, a 3-dimensional line-of-response (LOR) is defined along which the annihilation event occurred. Through the measurement of many such LORs, the position of the tracer can be determined with an associated uncertainty.

However, not all recorded LORs arise from true coincidence events. Random coincidences can occur when a photon originating from another unassociated source is detected within the coincidence window forming one or both parts of a coincident pair. Similarly, scattered LORs occur when one or both coincident photons scattered in surrounding materials before being detected. To account for these issues, an iterative least-squares minimisation algorithm [1] is used to remove corrupt LORs, finding the most likely location of the tracer at a given time.

The spatial resolution of a PEPT system operating as described can be estimated with $u(\bar{P}) = \frac{w}{\sqrt{T}}$ where $u(\bar{P})$ is the 3-dimensional location uncertainty on a measured PEPT location $\bar{P}$, w is the spatial resolution of the positron camera, and T is the true coincidence rate [6]. To approach micro-scale tracking, PEPT location uncertainty must be reduced, achieved by either reducing w or increasing T.

Considering significant changes to typical tracer choice and production to be beyond the scope of this work, reducing w can be achieved by reducing the pixel size of the detection system, and improving its energy resolution. Increasing T can be achieved by increasing the data rate, by increasing either the activity of the tracer or by increasing the absolute efficiency of the detection system. Absolute efficiency is determined by the intrinsic efficiencies of the detector materials and the geometric efficiency of the whole system, assuming no deadtime.

Typical PEPT systems have fixed geometries and detector materials implying fixed efficiencies, energy resolution, and pixel sizes. Significant improvements to the spatial resolution of a PEPT system are achieved with the development of a new detection system optimising these properties for micro-scale measurement, with an emphasis on reduced pixel size and increased energy resolution. Typically however, an improvement in energy resolution and pixel size is accompanied with reduction in absolute efficiency. A modular detection system allowing adjustment of its geometry and therefore absolute efficiency is ideal, and the use of multiple detection systems with different materials and properties as a hybrid camera allows for the highest degree of optimisation.

3. Detector technologies

Noting the significant dependence of the PEPT spatial resolution on pixel size and energy resolution, semiconductor detectors typically offer the best performance. Previous work [4] has investigated the feasibility of the University of Cape Town (UCT) Polaris system [7], consisting of a pair of pixelated room-temperature cadmium zinc telluride (CZT) semiconductor crystals shown in figure 1, with promising results demonstrating sub-millimeter tracking of low activity tracer particles [4].

However, the absolute efficiency and timing resolution of the semiconductor system are both relatively low, negatively impacting the achievable coincidence rates, and hence location frequency. The achievable FOV dimensions of the system were limited by the small detector scale, preventing its use in applications requiring micron precision where system scales are on the order of centimeters. To improve on the FOV scale and location rates, it is natural to turn to larger scintillator detectors, offering improved absolute efficiencies and timing resolutions.

UCT has detector components from a Siemens ECAT 951 and EXACT HR++ PET scanners retired from clinical use, both comprised of detector blocks of bismuth germanate oxide (BGO) segmented into 8x8 scintillator crystals, shown in figure 1. The detector blocks from the HR++

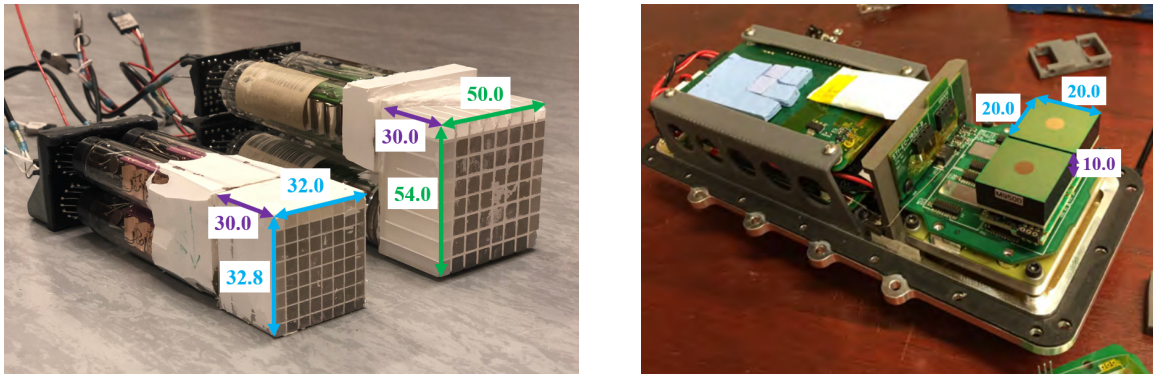

Figure 1. (Left) Detector blocks from the EXACT HR++ (left) and ECAT 951 (right) without protective casing. In each, four photomultiplier tubes and their 8x8 segmented crystals can be seen. (Right) The internals of the PolarisJ module, showing the two CZT crystals as the green squares on the right. All dimensions are given in mm.

camera are smaller than those from the 951, having pixel dimensions of 4.1 x 4.0 x 30 mm^3 and 6.75 x 6.25 x 30 mm^3 respectively, where the difference implies a trade-off between spatial resolution and absolute efficiency by virtue of their relative pixel densities and overall sizes.

Both of these detector types offer at minimum an intrinsic detection efficiency of 55% at 511 keV, whereas the Polaris system, with its much smaller pixels of 1.8 x 1.8 x 0.5 mm^3, offers only 15% detection efficiency. Through the development of a modular hybrid system, the trade-offs between all three detector types can be optimised for micro-scale tracking, achieving micro-scale location precision mostly through the use of the semiconductor system while maintaining useful location rates and larger volume FOV through the scintillators.

4. Detector characterisation

4.1. Energy resolution

Important elements of the PEPT detection system are the lower and upper level discriminators (LLD and ULD respectively), determining the allowed range of measured energy values describing a valid annihilation photon. Setting these limits accurately reduces noise by removing scattered events that are corrupt LORs. The energy resolution of the corresponding detector block is determined by measuring the width of the appropriate 511 keV photopeak. The energy resolution of a 951 detector block was determined in this paper, and similar calculations have been performed for both the HR++ blocks [8] and the Polaris system [4].

The four photomultiplier tubes (PMTs) from each detector block were connected to individual NIM pre-amplifiers and amplifiers, with the corresponding signal from each summed and digitised, using a multi-channel analyzer to produce pulse height spectra. However, since the detector PMTs do not provide uniform outputs due to manufacturing and component tolerances, a process of gain-matching was performed with photopeaks from each PMT aligned in pulse height by adjusting the gains of the separate amplifiers producing a single photopeak in the summed output.

Using three calibration sources, Na-22 (511 and 1275 keV), Cs-137 (662 keV) and Co-60 (1173 and 1332 keV)[9], an energy calibration was performed by Gaussian fitting to the appropriate photopeaks and relating them to their expected energies. Due to the poor energy resolution of the BGO crystals, the two independent photopeaks of the Co-60 source could not be separately identified as their Gaussian peaks overlapped, producing a larger single Gaussian peak. To account for this in the calibration, a single Gaussian was fit to the combined peak using a weighted mean centroid.

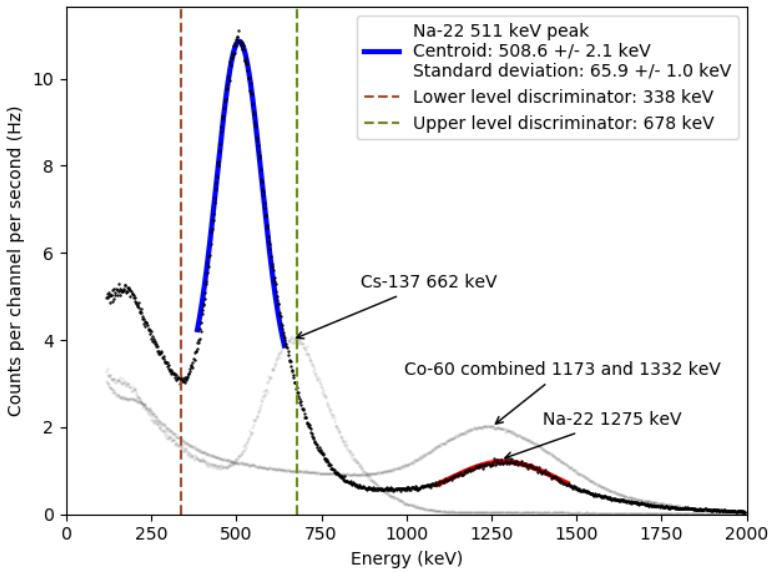

Figure 2. Calibrated energy spectra of the three sources as measured by a 951 detector block. The Na-22 spectrum is shown in bold, with Gaussian peaks fitted to each photopeak. Optimal lower and upper level discriminators are shown as dashed vertical lines.

The fitting parameters of the 511 keV peak of Na-22 were determined from figure 2 and the energy resolution was calculated to be $30.51 \pm 0.48\%$ at 511 keV. Repeating the process for the 1275 keV photopeak, an energy resolution of $28.9 \pm 2.2\%$ was found. Using the computed energy resolution, the optimal lower and upper level discriminators were selected to be the centroid energy $\mu \pm N\sigma$, where N was chosen to include 99% of the photopeak, giving 338.9 ± 3.3 keV and 678.4 ± 3.3 keV respectively. The LLD agrees with the expected energy of the Compton edge, indicating that this choice of N excludes the Compton scattered photons from the 511 keV peak, reducing the fraction of corrupt LORs.

4.2. Temporal resolution

The temporal resolution describes the precision at which the system can measure the time of arrival for a single detection event. Two single events are regarded as simultaneous, or coincident, if they both occur within a coincidence window of time period 2τ, where τ is limited by the time resolution in resolving an event. When 2τ is greater than the time resolution of the system, all true coincidences will be recorded, and the number of recorded random coincidences increases linearly with τ. Knowledge of the time resolution allows for the careful selection of 2τ which maximises the true coincidence rate while limiting the random coincidence rate, minimising the inclusion of corrupt LORs from random events.

Singles events were recorded for a positron source central to a pair of detector modules operating in coincidence, and a time delay was added to the events in one module. By varying this delay and determining the number of events that were within the same coincidence window, a Gaussian curve representing the system's coincidence timing resolution was plotted. As the delay is increased from zero, fewer true coincidences are detected and beyond a point all measured coincidences are random coincidences.

As the size of the coincidence window is increased beyond the system's intrinsic timing resolution, the Gaussian curves reach a maximum and plateau, having a flat top as all true

coincidences are fully covered by the chosen window. Increasing the coincidence window beyond that point leads to the inclusion of a higher fraction of corrupt LORs.

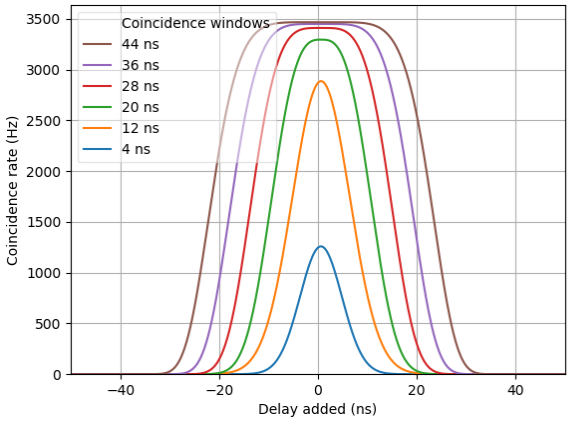

Figure 3. The coincidence rate as a function of time delay added to one of the coincident modules. Each curve represents a different coincidence window, 2τ.

In figure 3, these curves are shown for varying coincidence windows, with the flat top visible at large coincidence windows. Fitting a Gaussian function to each of the curves with coincidence windows of 4 and 12 ns, being the curves with typical Gaussian shapes, the FWHM of each was determined to be 9.98 ± 0.03 ns and 13.61 ± 0.03 ns respectively. The difference in these values arises from the use of different coincidence windows. In the 12 ns case, 2τ is greater than the time resolution of the system and the window width is included in the peak, whereas in the 4 ns case 2τ is less than the system's time resolution, being approximately 10 ns.

4.3. Geometry definition

The construction of the hybrid camera system needs to be carefully optimised to leverage the benefits of each detector type if it is to be used for micro-scale PEPT. A BGO part of the system consisting of two modules of four 951-series detector blocks and two modules of HR++ detector blocks was developed.

Clearly, the central region of the detector system is the most significant in measurements of micro-scale phenomena and the Polaris system must therefore be placed there. The placement of the BGO modules is then more flexible, and their individual characteristics have to be taken into account. To do this, a Monte Carlo simulation of the sensitivity profile of the system was used for further optimisation, where the Monte Carlo aspects of the code handled the volume effects of the crystals and their intrinsic efficiencies. A fairly uniform sensitivity profile is desired in the central region of interest to avoid dead time limiting hot spots and to allow uniformity of PEPT measurements over the volume, but absolute uniformity is difficult to achieve due to the number of detector types being used.

In figure 4, the geometry of the hybrid camera system is shown, consisting of 1024 BGO pixels and 9680 CZT pixels, giving a high resolution region of interest between the Polaris modules of $(62 \times 42 \times 20)$ mm^3 shown as a shaded red region, and a larger FOV between the BGO modules of $(150 \times 196 \times 101)$ mm^3. This geometry was selected as the HR++ blocks placed between the 951 blocks allow for the improved spatial resolution of the HR++ blocks to contribute significantly to the central region of interest, while also maintaining improved absolute efficiencies and an increased FOV as offered by the 951 blocks.

The uniformity of the sensitivity profile was validated using the simulation in figure 4, where sensitivity profiles as functions of their corresponding coordinates are shown at different depths along the Z axis in grey, with the mean sensitivity over all depths shown in bold. The uniformity

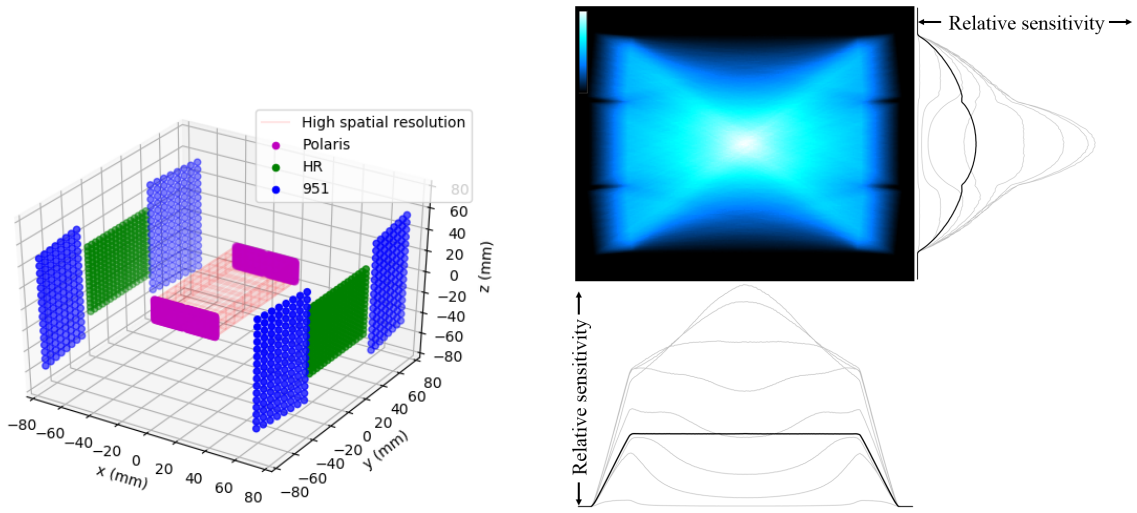

Figure 4. (Left) The geometry of the hybrid camera, showing each segmented detector element as a separate pixel with the central shaded high resolution region. (Right) The simulated sensitivity profile in the XY plane integrated along the Z axis, with corresponding profiles along the Y (side) and X (bottom) axis shown at varying depths. All profiles are drawn to scale.

of the central region can be seen in these profiles, although notable variation in uniformity can be seen at varying depths. Several other possible geometries were also tested, with none achieving similar central uniformity as in the chosen geometry.

5. Conclusions and future work

A modular BGO scintillator array was constructed to enable the application of PEPT to systems on the small scale, at micron precision. A numerical model of the sensitivity profile of the system was used to optimise the chosen geometry for uniformity within its field of view. Energy and timing resolutions were determined, allowing for the optimisation of system parameters for low noise detection. Precise characterisation of the detection efficiency, spatial resolution and deadtime parameters of the system in the future will lead into the development of a hybrid detector system combining the modular BGO array with a pair of high resolution pixelated semiconductor detectors, enabling the application of PEPT in the study of micro-scale phenomena for the first time.

References

[1] Parker D, Broadbent C, Fowles P, Hawkesworth M and McNeil P 1993 *Nuclear Instruments and Methods in Physics Research Section A: Accelerators, Spectrometers, Detectors and Assoc. Equipment* **326** 592 – 607
[2] Buffler A, Govender I, Cilliers J, Parker D, Franzidis J P, Mainza A, Newman R, Powell M and Van der Westhuizen A 2009 *Int. Topical Meeting on Nuclear Research Applications and Utilization of Accelerators*
[3] Leadbeater T, Parker D J and Gargiuli J 2012 *Particuology* **10**(2) 146–153
[4] Hyslop N 2021 *Sub-Millimetre Positron-Emission Particle Tracking Using a CdZnTe Semiconductor Array* Master's thesis
[5] Knoll G F 2009 *Radiation Detection and Measurement* (John Wiley) pp 12–13 3rd ed
[6] Leadbeater T and Parker D 2013 *7th World Congress in Industrial Process Tomography* pp 85–94 ISBN 0853163235
[7] H3D Inc. 2018 *J6400 High-Energy High-Flux Spectrometer* URL `https://h3dgamma.com/J6400Specs.pdf`
[8] McKnight A, Leadbeater T and van der Merwe R 2022 *Characterisation of a new LSO block detector for Positron Emission Particle Tracking* The Proceedings of SAIP2022
[9] NuDat database *National Nuclear Data Center* URL `https://www.nndc.bnl.gov/nudat/`